Lab on a Chip

PAPER

View Article Online
View Journal

Cite this: DOI: 10.1039/d6lc00135a

Centrifuge-free separation of plasma from milliliters of whole blood for point-of-care diagnostics

Christia M. Victoriano,[a] Bianca Arraiza Carlo,[b] Abigail G. Ayers,[a] Kelia A. Human[a] and Samuel K. Sia *[a]

Performing efficient plasma separation from whole blood, a vital sample matrix for diagnostics, in point-of-care settings remains challenging, particularly for sensitive assays that require larger volumes than can be obtained from a finger prick. Centrifugation, the gold standard for plasma separation, relies on bulky equipment and trained personnel, making it difficult to implement in decentralized settings. Current point-of-care (POC) plasma separation methods are limited to microliter blood volumes, which are insufficient for high-sensitivity clinical applications; these tools also require manual operation and yield limited plasma volumes. Here, we present PlasmaLIFT (Large-volume Immunodepletion and Filtration Tool), an automated and compact device that uniquely combines two plasma separation strategies—immunomagnetic red blood cell depletion that enables downstream filtration without clogging, and a dual membrane size-exclusion filtration recently developed that removes remaining cells—to enable rapid, efficient plasma separation from 5 mL of whole blood within 10 minutes. PlasmaLIFT removes over 99.9% of cellular components without needing significant dilution or causing hemolysis, achieves a high plasma recovery efficiency of 80% at physiological hematocrit levels, and produces plasma containing clinically relevant biomarkers—demonstrated here for proteins, metabolites, lipids, nucleic acids, and viruses—at levels comparable to those obtained with centrifugation. This scalable, automated, centrifuge-free approach facilitates high-volume plasma separation in decentralized settings, potentially expanding access to sensitive blood-based diagnostic testing; future work to reduce the cost of magnetic beads at scale will expand access even further to low-resource settings.

Received 11th February 2026,
Accepted 3rd April 2026

DOI: 10.1039/d6lc00135a

rsc.li/loc

Introduction

Blood is a critical sample matrix in clinical diagnostics, providing a rich source of molecular biomarkers[1] that enables assays spanning bloodborne pathogen detection and metabolic disorder screening, as well as liquid biopsy.[2] Unfortunately, efficient plasma separation from whole blood at the point of care (POC) remains a central challenge,[3–5] as centrifugation relies on bulky, expensive equipment and trained personnel. Even where low-cost, fixed-speed centrifuges are available, they often have low rotor speeds that can cause incomplete separation,[6,7] require longer spin times, are sensitive to rotor balance variations, handle only small volumes,[8] and demand careful manual pipetting without disturbing the cell pellet. Recent work[3,5,9,10] has identified plasma separation of larger volumes of whole blood as a particularly significant challenge for high-sensitivity assays at the POC. Both viral load testing for bloodborne pathogens and emerging liquid biopsy approaches[10] require large volumes of blood, due to the low abundance of biomarkers. Specifically, the GeneXpert assays for HIV, HBV, and HCV (which are intended for POC use) require 1 mL of plasma;[11] unfortunately, this requirement precludes rapid viral load testing in important settings like primary care clinics, harm reduction centers, prisons, rural clinics, and sexual health facilities, which lack the laboratory infrastructure needed to prepare plasma samples from whole blood for testing.[12]

Importantly, even when downstream analysis is performed at centralized laboratories, plasma separation at the point of collection remains critical for preserving sample integrity. Transporting whole blood introduces both logistical and biological challenges, as unprocessed blood is biochemically unstable and must be maintained under controlled conditions (typically 2–8 °C) to limit hemolysis and analyte degradation. Hemolysis – a leading cause of sample rejection[13] – releases intracellular components that can skew analyte levels and

[a] Department of Biomedical Engineering, Columbia University, New York, NY 10027, USA. E-mail: ss2735@columbia.edu
[b] Department of Biomedical Engineering, Harvard University, Cambridge, MA 02138, USA

inhibit assays,[9,14,15] while ongoing metabolism can alter analyte concentrations (*e.g.*, glucose decreases by 5–7% per hour).[16,17] Accordingly, guidelines recommend plasma separation within hours of collection,[18] and studies show that immediate separation reduces hemolysis, analyte degradation, and sample rejection compared to delayed processing.[19–21] Thus, POC plasma isolation not only enables decentralized testing but also improves the reliability of samples destined for centralized analysis.

As such, numerous methods are being developed for POC plasma separation, based on microfluidics, membrane filtration, capillary action, and sedimentation. However, these methods are often limited to small volumes (<100 μL); they cannot scale to milliliter volumes without introducing significant clogging of RBCs and/or low, inconsistent plasma yields.[22–34] To mitigate clogging, many previous methods required substantial dilution of whole blood, thereby reducing the concentration of target analytes and potentially leading to impractically large volumes for downstream assays. Although some systems can handle slightly larger volumes (200 μL to 1.8 mL), they often yield low plasma volumes and require manual handling, posing concerns regarding reproducibility and biosafety, especially in settings with minimally trained users (Table S1).[35–38] Currently, processing milliliters of whole blood into cell-free plasma remains challenging in POC settings. A recent review article on whole-blood separation techniques notes that there still lacks a technique with demonstrated robustness across all relevant biomarker classes, or a user-friendly procedure that performs consistently across hematocrit levels and sample volumes encountered in real-world use, such as in the POC.[4]

To process whole blood at the POC, our group recently developed a dual-membrane syringe filter to sequentially filter blood cells, which was integrated with microfluidic nucleic-acid extraction.[39] The design features two stacked glass-fiber membranes of progressively smaller pore sizes to

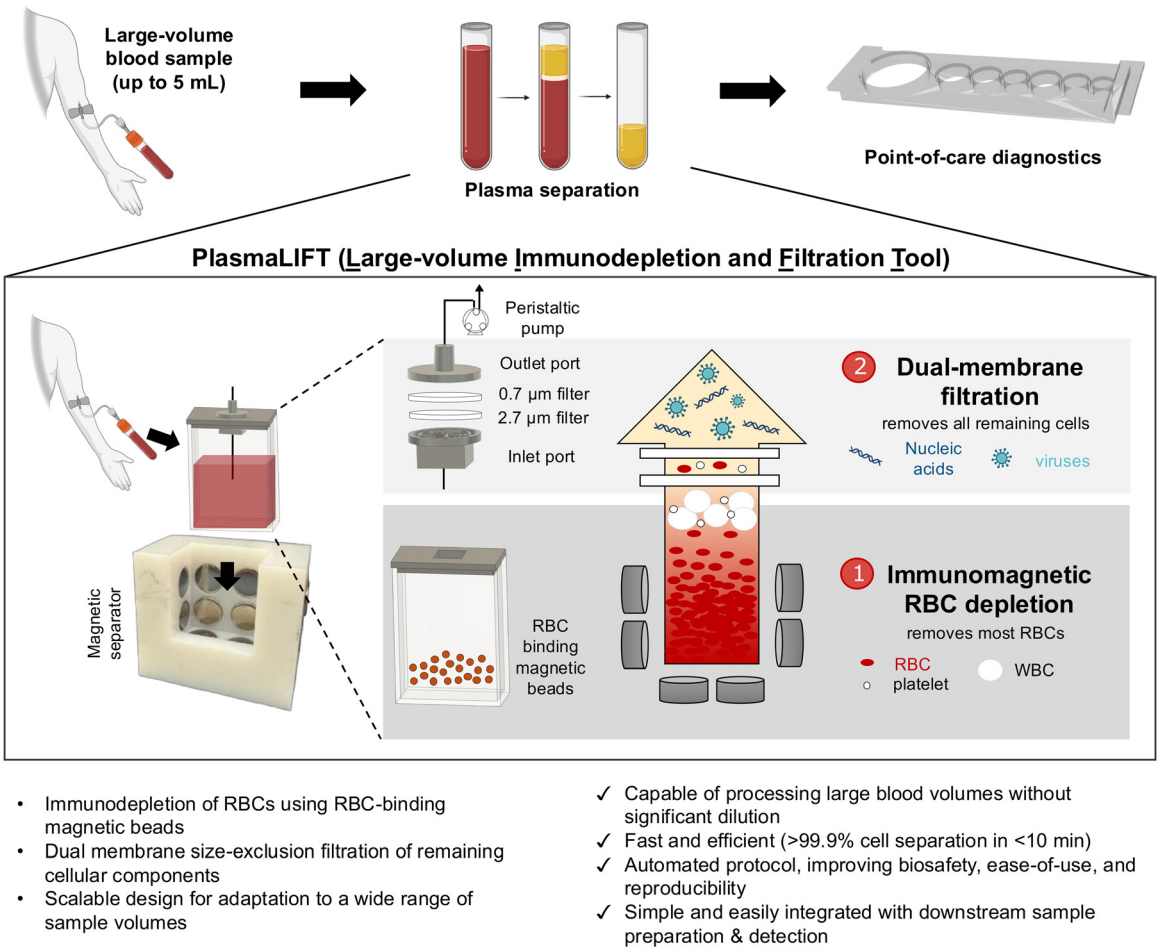

Fig. 1 PlasmaLIFT enables rapid, automated plasma separation from up to 5 mL of whole blood by combining RBC immunomagnetic depletion with dual-membrane size-exclusion filtration. The system consists of a sample chamber preloaded with anti-RBC magnetic beads and a filter cap containing two glass-fiber membranes. After blood is added, the chamber is sealed, gently mixed, and placed in a magnetic separator. Bead-bound RBCs are pulled to the chamber walls, and a peristaltic pump draws the RBC-depleted supernatant through the filter cap; the RBC depletion step allows filtration to take place without clogging. In the second step, filtration removes cells while retaining diverse classes of analytes of interest. PlasmaLIFT produces large plasma volumes in under 10 min, with minimal clogging, hemolysis, or dilution, and is compatible with on-site testing, stable sample transport, and downstream automated workflows.

avoid the clogging caused by blood components on a single filter. The dual-membrane filter can process 50 μL of blood with low hemolysis and high virus recovery; however, scaling to milliliter volumes may require impractically large filters and the large dilution of analytes to prevent RBC clogging. To address these limitations, we develop PlasmaLIFT (Large-volume Immunodepletion and Filtration Tool), a simple device requiring no user intervention after initial steps (*i.e.* adding sample and placing on magnetic separator) for performing large-volume plasma separation at the POC. PlasmaLIFT combines this recently demonstrated dual membrane size-exclusion filtration approach with initial immunomagnetic depletion of RBCs (Fig. 1). A previous elegant approach by the Erickson group used RBC-binding magnetic beads to remove RBCs from whole blood[40,41] as a means of cell separation, but did not focus on downstream biomarker analysis where the retained white blood cells and platelets could contaminate the sample matrix with DNA, RNA, and proteins. The PlasmaLIFT approach hypothesizes that integrating the depletion of RBCs ahead of filtration—where filtration removes remaining cells—can increase the volume capacity of whole blood that can be processed by the filter; the combination of both steps can yield milliliters of plasma free of cells, in which biomarkers across diverse classes are demonstrated to be retained with high yield.

Results

PlasmaLIFT design and workflow

PlasmaLIFT comprises three main device components: (1) a single-use, disposable sample chamber and dual-membrane filter cap, (2) a reusable magnetic separator containing an array of permanent magnets, and (3) a peristaltic micropump connected to a laptop or microcontroller for automated operation (Fig. 2A and S3). The sample chamber is pre-loaded with magnetic particles functionalized with antibody complexes recognizing glycophorin A, a major sialoglycoprotein found in the membrane of human RBCs, designed to enable immunomagnetic depletion of RBCs using the magnetic separator. The filter cap consists of parallel glass fiber membranes of progressively smaller pore sizes (2.7 μm and 0.7 μm from bottom to top) (adapted from the dual membrane syringe filter approach previously developed by our group).[39] The filter cap seals the sample chamber and, through attached stainless steel tubing at the inlet and outlet, enables integrated, in-line filtration of RBC-depleted supernatant into cell-free plasma (removing residual RBCs, WBCs, platelets, and magnetic beads) using a peristaltic micropump, without manual sample transfer steps.

The circular peristaltic micropump (CPP-11000-ZM, Jobst Technologies) is compact, with a cubic volume of ~4 cm^3 (1/5000th the volume of a benchtop microcentrifuge capable of processing 5 mL tubes). Hence, it fits easily into decentralized POC settings, such as doctors' offices and pharmacies. It delivers low flow rates (5 μL to 1600 μL min^{-1}) and operates at a maximum of 3.3 V, with the flow rate proportional to the applied voltage. In the future, this low-power design could enable straightforward adaptation for battery-powered control, allowing for field operation in settings without grid-based power.

The device workflow is shown in Fig. 2B. Blood is first added by the user *via* syringe to the sample chamber containing anti-RBC magnetic beads, sealed using the filter cap, and gently mixed by the user (*via* brief, gentle inversion of the sample chamber). The user then attaches the pump tubing to the filter cap, places the sample chamber into the magnetic separator, and presses "start." Once placed into the magnetic separator, the magnetic-particle-bound RBCs are drawn to the permanent magnets on the bottom, back, and sides of the sample chamber ("lifting" RBC-depleted plasma to the top and front of the chamber). After a short incubation period, the peristaltic pump activates, and the RBC-depleted plasma is drawn through the dual-membrane filter cap into an empty sample tube, yielding cell-free plasma for immediate on-site testing or sample transport.

Initial testing of immunomagnetic red blood cell depletion with filtration

PlasmaLIFT is designed to integrate immunomagnetic depletion of RBCs with dual membrane size-exclusion filtration, efficiently removing cellular components from large volumes of whole blood without clogging, hemolysis, or substantial dilution. Given that RBCs are the most abundant cellular component in blood (comprising 40–45% of blood volume, with ~4–6 million RBCs per microliter), we hypothesized that front-end depletion of a substantial fraction of RBCs, before the sample encounters the membrane, would improve filtration efficiency and expand the system's practical volume capacity relative to filtration alone.

Using the filter alone, processing 5 mL of whole blood resulted in low plasma yield (mean = 45 μL) due to rapid membrane clogging, which halted flow (Fig. 2C). In contrast, when RBCs were first immunomagnetically depleted and the partially cleared sample was subsequently passed through the dual-membrane filter, plasma yield increased significantly (1.96 mL, $p < 0.0001$). To determine whether immunomagnetic depletion alone could sufficiently separate cellular components, we evaluated RBC separation efficiency in isolation. Although this step enabled ~1000-fold depletion, it still left, on average, 4878 cells μL^{-1} in the recovered plasma (Fig. 2D). Notably, only when depletion and filtration were combined did residual cell levels fall sharply (mean = 56 cells per μL). This data suggests that the combined depletion-filtration approach, rather than either component alone, is essential for achieving high-quality plasma isolation from larger input volumes.

Optimization of immunomagnetic depletion of red blood cells

To enable PlasmaLIFT for diagnostic applications that require large plasma volumes, we first optimized workflow and design parameters to maximize plasma yield. The efficiency of

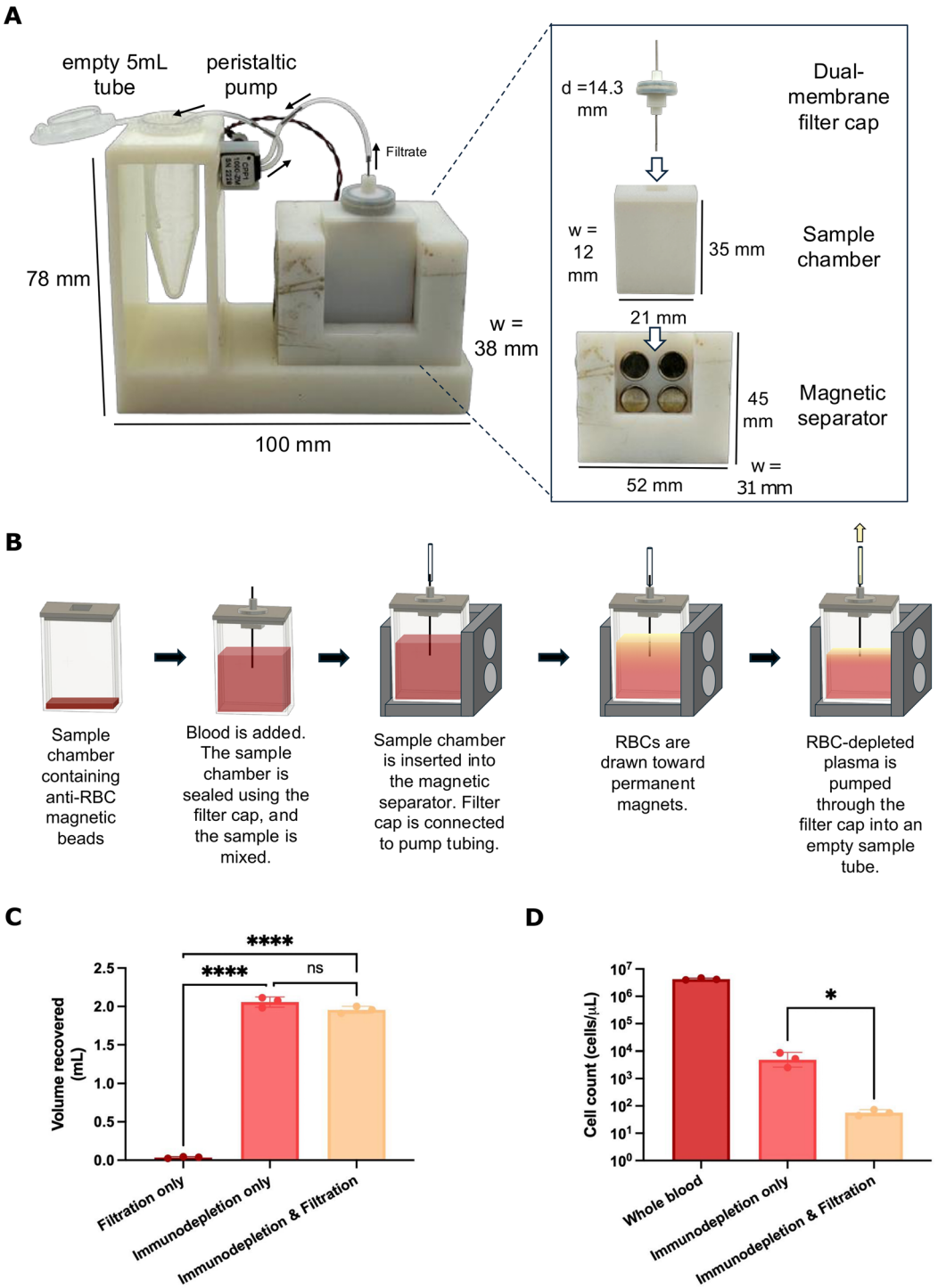

Fig. 2 PlasmaLIFT workflow and initial testing. (A) The core components of PlasmaLIFT comprise a magnetic separator, a sample chamber, and a dual-membrane filter cap. The filter cap is designed to seal the lid of the sample chamber. The sample chamber is designed to fit snugly into the magnetic separator, in direct contact with the magnets, securely holding the sample and maximizing the magnetic field applied to the chamber. Tubing connected to the filter cap outlet connects to the inlet of a miniature peristaltic pump. Outlet tubing connected to the peristaltic pump is inserted into an empty 5 mL tube. The peristaltic pump automates the flow of the filtrate from the sample chamber through the filter and into the empty sample tube. The peristaltic pump is connected to a laptop (not shown) and controlled by the pump's driver software. (B) PlasmaLIFT workflow. Blood is dispensed into the sample chamber, sealed with a filter cap, and gently mixed. The chamber is then placed in the magnetic separator and connected to a peristaltic pump. Bead-bound RBCs are captured by the magnets, and the resulting RBC-depleted supernatant is pumped through the filter cap into a collection tube or downstream preparation device. (C) Volume yield for blood processed by filtration, immunomagnetic depletion, and combined depletion and filtration. Filtration alone recovered only ~45 μL due to rapid membrane clogging; immunomagnetic depletion and combined processing yielded 2.06 mL and 1.96 mL on average, respectively. (D) Cell separation efficiency for RBC immunodepletion with and without filtration. Immunodepletion alone resulted in 4878 cells per μL, while the addition of dual-membrane filtration produced a nearly 87-fold further reduction to 56 cells per μL.

immunomagnetic RBC depletion depends on the geometry of the sample chamber and configuration of the magnetic separator. Effective magnetic separation requires a magnetic field that is sufficiently strong and spatially optimized to rapidly isolate RBCs from the entire chamber, while maintaining a distinct plasma zone for extraction that is largely free from RBC-bound magnetic beads. Hence, we designed and evaluated three chamber and magnetic separator prototypes to evaluate the speed and spatial resolution of magnetic separation. Finite element modeling (COMSOL) was used to simulate the applied magnetic field on the chamber for each prototype, followed by validation through visual observation of RBC separation (Fig. S1). Across all designs, observed RBC migration correlated well with regions of high magnetic field strength, while RBC-depleted plasma accumulated in areas of low field strength.

In an initial vertical configuration (Fig. S1), testing resulted in two separate plasma accumulation zones due to uneven magnetic field distribution; this result would complicate automation where plasma must be drawn from a single fixed point. In addition, the vertical orientation also resulted in slower RBC separation from the upper chamber regions. We designed a horizontal configuration (Fig. S1), which improved separation kinetics but offered only a limited plasma accumulation area near the chamber front. By contrast, a nearly square-chamber geometry (Fig. S1) demonstrated the most effective separation performance, enabling both rapid RBC clearance and a clearly defined plasma collection zone. Quantitative analysis of RBC-depleted supernatant recovery after 5 minutes of magnetic separation confirmed the superior performance of the square-chamber geometry, which yielded 1.990 mL of supernatant, compared to 1.696 mL and 1.348 mL for the vertical and horizontal configurations, respectively (Fig. S2A). The square-chamber configuration also demonstrated the most efficient RBC separation, with 3233 remaining cells per μL in the supernatant, compared to 53 417 and 17 624 cells per μL for the vertical and horizontal configurations, respectively (Fig. S2B). Based on these results, we selected the square-chamber configuration for further PlasmaLIFT development.

To further improve immunomagnetic RBC depletion, we evaluated the effect of changing the volume of anti-RBC magnetic beads added per milliliter of whole blood. We tested a range of bead concentrations from 50 to 150 μL beads per mL blood and measured the corresponding RBC-depleted supernatant recovery (Fig. 3A). Supernatant yield increased with bead volume; however, the improvement

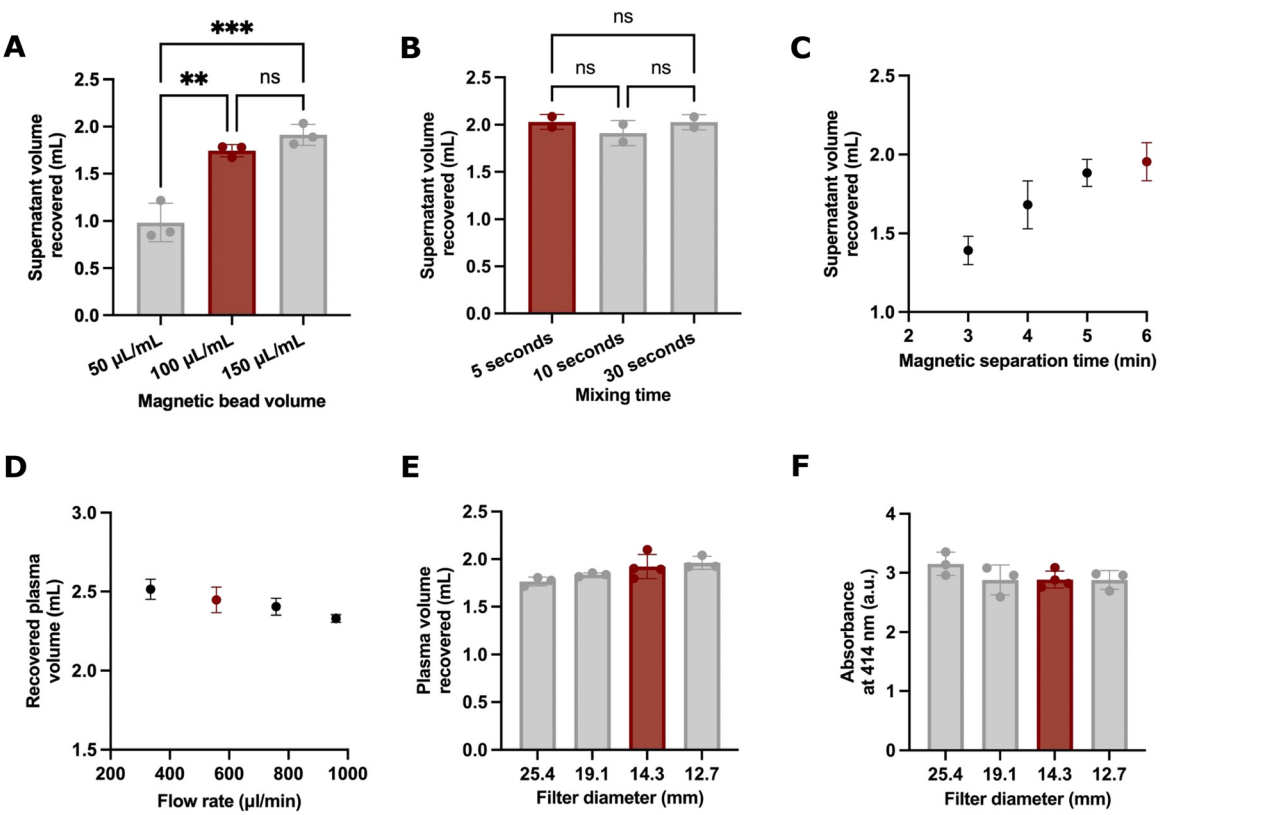

Fig. 3 Optimization of workflow and design parameters. (A) Optimization of magnetic bead volume. Supernatant recovery increases with bead volume, plateauing beyond 100 μL beads per mL blood. (B) Varying mixing time does not have a significant effect on supernatant yield. (C) Optimizing magnetic separation time. Yield increases up to ~5 minutes and then plateaus; 6 minutes was selected to balance yield and protocol duration. (D) Optimization of flow rate. Plasma recovery decreases with increasing flow rate; 557 μL min^{-1} was selected to balance yield and processing time. (E) Varying filter diameter does not have a significant effect on plasma yield. (F) Hemolysis is not significantly affected by filter diameter. Red datapoints/bars indicate selected design parameters. Error bars represent mean ± SD. ****$p < 0.0001$, ***$p < 0.001$, **$p < 0.01$, *$p < 0.05$.

plateaued beyond 100 μL mL^{-1}, with no statistically significant difference between 100 and 150 μL mL^{-1} (p = 0.3625). Based on this analysis, we selected 100 μL mL^{-1} as the optimal bead concentration for the PlasmaLIFT workflow.

We next assessed the impact of mixing time on plasma yield. Mixing whole blood with anti-RBC magnetic beads is the only manual step in the PlasmaLIFT workflow and thus a potential source of user-to-user variability. To evaluate the robustness of this step, we compared the yield of RBC-depleted supernatant after mixing for 5, 10, or 30 seconds. No statistically significant differences were observed among the groups (p = 0.4935; Fig. 3B), indicating that plasma recovery is insensitive to moderate variations in mixing time.

To reduce total protocol time while maintaining high plasma yield, we evaluated different times for the magnetic separation step, ranging from 3 to 6 minutes. Plasma yield increased with longer separation times, though differences beyond 3 minutes were not statistically significant. Based on the observed trend and yield plateau beyond 6 minutes (Fig. 3C), we selected 6 minutes as the optimal magnetic separation time.

Optimization of dual-membrane filtration and plasma removal

With the immunomagnetic RBC depletion step established, we sought to optimize its integration with the dual-membrane filtration process. First, we aimed to tune the pump flow rate to achieve a high plasma yield quickly. We evaluated plasma yield across voltages corresponding to flow rates of 335, 557, 758, and 960 μL min^{-1}, following 6 minutes of magnetic separation (Fig. 3D).

We observed that higher flow rates result in reduced plasma recovery (*i.e.*, negative correlation between flow rate and plasma yield, with R^2 = 0.71, p = 0.008), although no differences were observed among pairs of individual flow rate groups (one-way ANOVA, p = 0.13). Based on these results, we selected a flow rate of 557 μL min^{-1} (corresponding to 1.8 V) to achieve high plasma recovery and complete the entire process (including magnetic separation and filtration) in under 10 minutes (a typical duration of centrifugation protocols).

We then investigated the impact of reducing filter membrane diameter on plasma yield. Although smaller diameters reduce membrane surface area and potentially increase the risk of RBC clogging, this effect may be reduced due to upstream immunomagnetic depletion of RBCs. We tested a range of filter diameters, from 25.4 mm (used in our original dual-membrane filter design) down to 12.7 mm, and evaluated both plasma volume recovery and hemolysis, by measuring absorbance at 414 nm, the characteristic peak for free heme released from lysed blood cells. We observed a slight negative linear correlation between filter diameter and plasma yield (R^2 = 0.52, p = 0.0052), consistent with the hypothesis that reducing filter diameter increases plasma yield, but no differences in recovered plasma volume between individual filter diameter groups *via* one-way ANOVA (p = 0.778; Fig. 3E). Hemolysis did not differ significantly across diameter groups (p = 0.2294; Fig. 3F). Hence, we selected a 14.3 mm membrane diameter for further studies to achieve high plasma yield with low RBC clogging.

We characterized the pressure drop across the 14.3 mm dual membrane filters at the selected 557 μL min^{-1} flow rate. Transmembrane pressure was measured over time using a positive-pressure configuration (Fig. S3). Pressure increased gradually during filtration, reaching ~34 kPa (~4.9 psi) at the standard operating endpoint of 4 minutes. This gradual rise is consistent with progressive accumulation and embedding of red blood cells within the membrane. Beyond 4 minutes, pressure increased sharply, reaching ~140 kPa (~20 psi), indicative of the onset of membrane fouling and clogging. These results suggest that under typical operating conditions, the system operates within a moderate pressure regime prior to the onset of nonlinear resistance increases associated with filter saturation.

Evaluation of volume recovery, blood cell separation, and hemolysis

After selecting the device design and workflow parameters, we evaluated the plasma yields from PlasmaLIFT *vs.* centrifugation. From an initial blood volume of 5 mL, PlasmaLIFT recovered an average of 2.12 mL of plasma, compared to 2.64 mL from centrifugation ($p < 0.0001$), corresponding to an average plasma volume recovery efficiency of 80.3% (Fig. 4A). To assess plasma quality, we next compared the residual cellular content of plasma obtained by PlasmaLIFT and centrifugation. The PlasmaLIFT device achieved high blood cell removal efficiency (>99.999%), yielding an average residual cell count of 19.3 cells per μL, with no significant difference from centrifuged plasma (19.0 cells per μL; $p > 0.999$), from an initial whole blood concentration of 4.26×10^6 cells per μL (Fig. 4B). We also evaluated hemolysis by measuring absorbance at 414 nm. Plasma separated by the PlasmaLIFT device exhibited minimal hemolysis (2.24 a.u.), with no significant difference compared to centrifugation (2.11 a.u.; p = 0.2321) (Fig. 4C).

Evaluation of plasma separation across hematocrit levels

To evaluate the performance of PlasmaLIFT under physiologically relevant conditions, we validated the device across a range of hematocrit (HCT) levels. Hematocrit, the volume fraction of RBCs in whole blood, varies widely between individuals and can significantly impact the degree of RBC clogging in microfluidic and filtration-based systems.[25,39] Hematocrit typically ranges from 35–45% in healthy females and 39–50% in healthy males and can be further altered by factors such as hydration status, anemia, polycythemia, or underlying disease.[42] We thus evaluated plasma yield and hemolysis for blood samples with hematocrit levels ranging from 40–55%, which are at and beyond the normal physiological range.

As expected, we observed that higher hematocrit levels reduce the plasma fraction in whole blood (Fig. 4D, showing

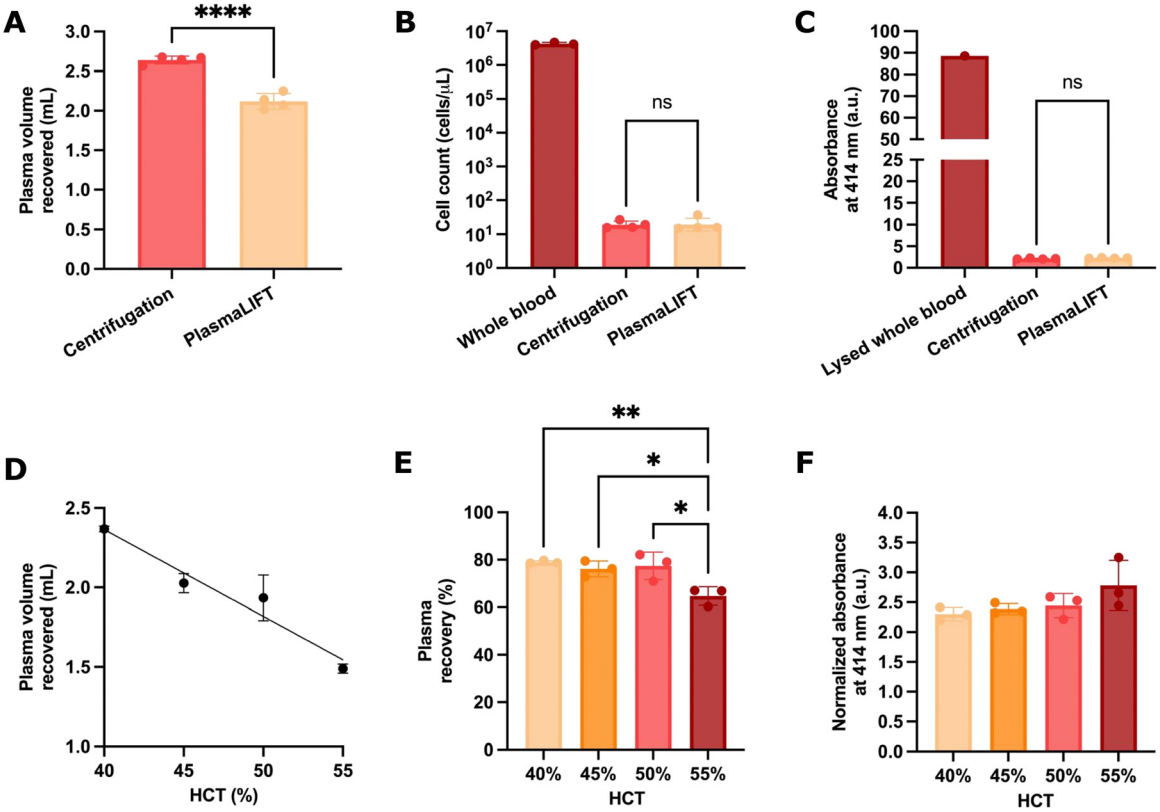

Fig. 4 Evaluation of plasma yield, cell separation efficiency, and hemolysis using PlasmaLIFT. (A) Plasma volume recovery for PlasmaLIFT *vs.* centrifugation. PlasmaLIFT yielded 2.12 mL on average *vs.* 2.64 mL for centrifugation ($p < 0.001$), corresponding to an 80.3% recovery efficiency. (B) Residual cell counts in separated plasma. PlasmaLIFT and centrifugation yielded comparable cell counts (19.3 *vs.* 19.0 cells per μL; $p > 0.999$), reflecting >99.999% filtration efficiency from an initial 4.26×10^6 cells per μL in whole blood. (C) Hemolysis comparison (absorbance at 414 nm). PlasmaLIFT and centrifugation yielded similar values (2.24 *vs.* 2.11 a.u., $p = 0.2321$). (D) Recovered plasma volumes across hematocrits (40–55%). Plasma yield decreased linearly with increasing hematocrit ($R^2 = 0.91$; $p < 0.0001$). (E) Plasma recovery efficiency by hematocrit. Efficiencies were 79.0%, 76.1%, 77.4%, and 64.7% for HCT levels of 40%, 45%, 50%, and 55%, respectively. Recovery did not differ significantly among 40–50% HCT but was reduced at 55% ($p = 0.0086$–0.0287). (F) Degree of hemolysis observed in plasma across hematocrit levels. No significant differences in hemolysis were observed across hematocrit levels ($p = 0.5007$). Error bars in all figures indicate mean ± standard deviation. ****$p < 0.0001$, ***$p < 0.001$, **$p < 0.01$, *$p < 0.05$.

a negative linear correlation between hematocrit and plasma yield from the PlasmaLIFT device ($R^2 = 0.91$; $p < 0.0001$)). Across HCT levels, plasma recovery efficiencies were significantly different ($p = 0.0074$). *Post hoc* multiple comparisons revealed that plasma recovery efficiency did not differ significantly between the 40% and 45% groups (79.0% and 76.1%, $p = 0.8052$), 40% and 50% groups (79.0% and 77.4%, $p = 0.9587$), and 45% and 50% groups (76.1% and 77.4%, $p = 0.9755$). However, the 55% hematocrit group demonstrated a slight decrease in recovery efficiency (64.7%) compared to the 40%, 45%, and 50% groups ($p = 0.0086$, 0.0287, and 0.0165, respectively) (Fig. 4E). There were no significant differences in hemolysis across hematocrit levels ($p = 0.5007$) (Fig. 4F).

Protein, metabolite, and lipid yield

To validate the quality of plasma produced by the separation device, we assessed the recovery of representative plasma components (proteins, lipids, and metabolites) in device-separated plasma compared to plasma obtained *via* centrifugation. Accurate recovery of these components is essential to ensure that the immunomagnetic depletion and filtration system does not significantly retain or adsorb specific biomolecules during plasma separation.

As an initial assessment, we measured total protein concentration as a broad indicator of plasma protein retention. The mean total protein concentration in PlasmaLIFT-separated plasma was 3.20 g dL^{-1}, which was not significantly different from that of centrifuge-separated plasma (3.30 g dL^{-1}; $p = 0.5337$) (Fig. 5A).

Next, we evaluated metabolite preservation by measuring glucose concentration in plasma separated by both the device and centrifugation. Glucose was selected as a representative metabolite due to its high clinical relevance and its routine use as a biomarker in plasma-based diagnostics. Accurate glucose measurement is crucial for diagnosing and managing diabetes, as well as for detecting acute metabolic disturbances, including hypoglycemia and hyperglycemia. We observed no significant difference in glucose levels between centrifuged plasma (18.70

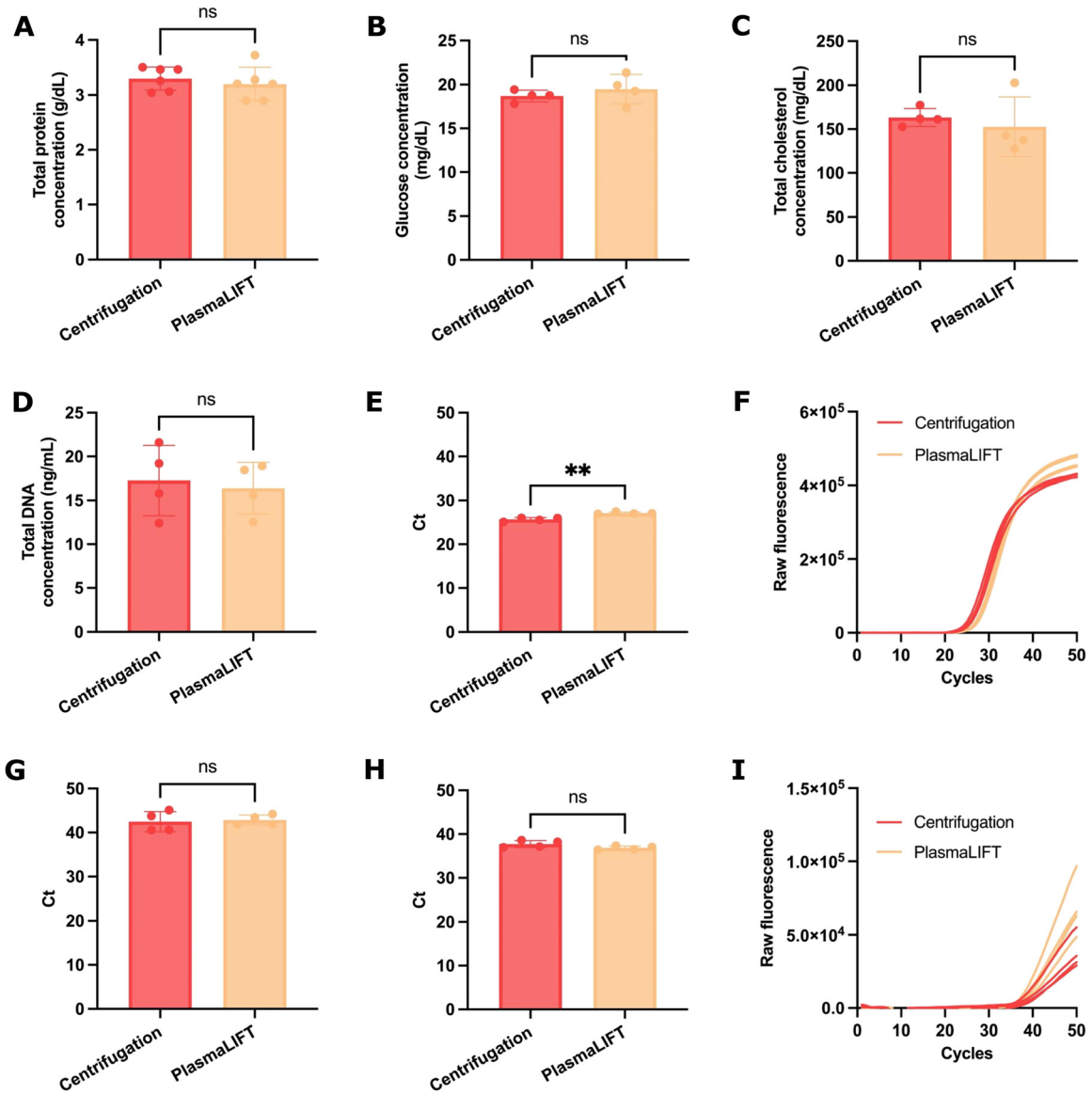

Fig. 5 Measurement of biomarker yield across diverse classes using PlasmaLIFT compared to centrifugation. (A) Total protein yield was comparable between PlasmaLIFT and centrifugation (3.20 *vs.* 3.30 g dL^{-1}; $p = 0.5337$). (B) Recovered glucose levels were comparable between PlasmaLIFT and centrifugation (19.46 *vs.* 18.70 mg dL^{-1}; $p = 0.4407$). (C) Total cholesterol concentrations between PlasmaLIFT and centrifugation did not differ significantly (152.7 *vs.* 163.3 mg dL^{-1}; $p = 0.5725$). (D) Total endogenous DNA yield was comparable (16.4 *vs.* 17.3 ng mL^{-1}; $p = 0.7371$). (E) qPCR detection of a 179-bp spike-in DNA fragment showed a slight Ct delay for PlasmaLIFT *vs.* centrifugation (27.1 *vs.* 25.7 cycles; $p = 0.022$). (F) Corresponding qPCR fluorescence curves show a modest delay in amplification for PlasmaLIFT. (G) RT-qPCR detection of spike-in cel-miR-39 showed similar Ct values for PlasmaLIFT compared to centrifugation (42.8 *vs.* 42.5 cycles; $p = 0.7972$). (H) RT-qPCR detection of spike-in inactivated HCV RNA showed no significant Ct difference for PlasmaLIFT compared to centrifugation (36.8 *vs.* 37.7 cycles; $p = 0.1115$). (I) Fluorescence curves for HCV detection show no amplification delay, indicating comparable viral recovery. Error bars in all figures indicate mean ± standard deviation. $^{****}p < 0.0001$, $^{***}p < 0.001$, $^{**}p < 0.01$, $^{*}p < 0.05$.

mg dL^{-1}) and device-separated plasma (19.46 mg dL^{-1}, $p = 0.4407$) (Fig. 5B).

Finally, we assessed lipid preservation by measuring total cholesterol concentration, a standard clinical biomarker used to evaluate cardiovascular risk. This measurement requires preservation of both free and lipoprotein-bound cholesterol. Again, no significant difference was observed between centrifuged plasma (mean concentration = 163.3 mg dL^{-1}) and device-separated plasma (152.7 mg dL^{-1}; $p = 0.5725$) (Fig. 5C).

Nucleic acid recovery

We then sought to assess the compatibility of the PlasmaLIFT device with downstream applications involving cell-free nucleic acid detection, such as liquid biopsy. As cell-free nucleic acids are often present in plasma at very low concentrations, efficient recovery from large sample volumes is vital. We conducted experiments to measure the recovery of both endogenous and spiked nucleic acids in the separated plasma. Specifically, we

evaluated total cell-free DNA yield as an indicator of analyte preservation, along with recovery of spiked synthetic nucleic acids and microRNAs (miRNAs) to assess retention and loss during processing.

No significant difference was observed in total DNA recovery between centrifuged plasma (mean concentration = 17.3 ng mL^{-1}) and device-separated plasma (16.4 ng mL^{-1}; p = 0.7371) (Fig. 5D). To evaluate the recovery of spiked DNA, a 179-bp fragment of the bacteriophage lambda genome was spiked into whole blood samples prior to plasma separation. Quantitative PCR (qPCR) analysis revealed a slight delay in cycle threshold (Ct) values between plasma obtained by conventional centrifugation (25.7 cycles) and PlasmaLIFT (27.1 cycles, p = 0.022) (Fig. 5E). Similarly, qPCR fluorescence curves demonstrated ~1.4 cycle delay between the two methods (Fig. 5F).

To evaluate miRNA recovery, a quantified synthetic miRNA, cel-miR-39, was spiked into whole blood samples prior to plasma separation. No significant difference in Ct was observed between centrifugation (Ct = 42.5) and PlasmaLIFT (Ct = 42.8, p = 0.7972) (Fig. 5G).

Virus recovery from spiked blood samples

To evaluate the suitability of PlasmaLIFT for downstream applications involving viral pathogen detection and quantification, we assessed the recovery of inactivated hepatitis C virus (HCV) spiked into whole blood prior to plasma separation. Quantitative RT-PCR (RT-qPCR) analysis revealed no significant difference in cycle threshold (Ct) values between plasma obtained by conventional centrifugation (Ct = 37.7) and that separated using PlasmaLIFT (Ct = 36.8; p = 0.1115) (Fig. 5H). Similarly, RT-qPCR fluorescence curves showed no amplification delay between the two methods, indicating comparable efficiency in recovering viral particles during plasma separation (Fig. 5I).

Discussion

With increased development of lab-on-a-chip and other POC diagnostic devices, POC plasma separation is currently recognized as a major challenge.[4] We present PlasmaLIFT, a simple and compact plasma separation device that presents a novel strategy of combining immunomagnetic RBC depletion with a dual-membrane filtration design (recently demonstrated to work upstream of microfluidic nucleic acid extraction) to isolate milliliters of plasma from whole blood. Although previous studies have demonstrated variations of one of the two strategies in isolation, they were limited to processing small volumes or did not address the removal of white blood cells and platelets which could interfere with analysis of proteins or nucleic acids. By combining these two approaches, PlasmaLIFT can process milliliters of whole blood, substantially higher than existing POC devices (*e.g.*, under 1.8 mL with low plasma volume recovery),[37] achieving high plasma yield, high blood cell separation efficiency, and minimal cell lysis, comparable to centrifugation. The system yields ~2 mL of plasma from 5 mL of whole blood (~80% plasma recovery) at physiological hematocrit levels without significant dilution (The ~20% reduction in plasma recovery compared to centrifugation is primarily due to plasma retained within the magnetically compacted red blood cell fraction during depletion, with a smaller contribution from dead volume in the filtration module; both sources of volume loss can be reduced in the future through improved designs of chamber and magnetic field configuration). Importantly, this volume meets the requirements for several molecular diagnostic assays, including the Cepheid GeneXpert Viral Load tests for HIV, HBV, and HCV, as well as the Cobas EGFR Mutation Test v2. At very high hematocrit (>55%), the volume of plasma recovery was slightly reduced, but the quality of the plasma remained uncompromised, suggesting that the device is also suitable for use in patients with elevated hematocrit, including those with polycythemia, dehydration, or other atypical conditions. Plasma separated using PlasmaLIFT contains similar concentrations of analytes from a wide range of relevant biomarker classes to plasma obtained from centrifugation, as demonstrated for proteins, metabolites, lipids, nucleic acids, and bloodborne pathogens.

PlasmaLIFT is currently designed for POC settings that have access to routine blood draws but lack dedicated on-site laboratory space, instrumentation, or trained laboratory personnel, including primary care clinics, community health centers, urgent care facilities, rehabilitation and addiction centers, correctional facilities, and nursing homes. In these environments, PlasmaLIFT enables rapid on-site plasma preparation either for transport to centralized laboratories, improving sample stability and quality, or for immediate on-site testing with commercially available plasma-based POC assays, such as the Cepheid GeneXpert tests for HIV, HBV, and HCV. PlasmaLIFT can thus operate as a standalone POC tool or be integrated with microfluidic sample-preparation platforms for on-chip nucleic acid extraction. The largely automated workflow enhances biosafety and usability, reduces variability associated with manual handling, and can be adapted for battery-powered operation *via* a microcontroller. An integrated system with miniaturized electronics is estimated to occupy ~10 × 10 × 8 cm, substantially smaller than a typical benchtop centrifuge (~23 × 23 × 36 cm) (Fig. S4). Although the current workflow includes a brief manual mixing step, we found this operation to be robust to variation in mixing duration and easily performed by simple chamber inversion, with straightforward paths to automation *via* controlled mechanical agitation. In addition, the scalability of PlasmaLIFT to different sample volumes allows it to be potentially used with user-friendly blood self-collection devices (such as OnFlow and MaxFlow, RedDrop One, and Tasso), to expand use to even more remote POC settings without the current capability to perform venous blood draws.

There are a few current limitations of the system. The use of antibody-coated magnetic beads suspended in liquid introduces a very slight dilution (1.1×) and requires refrigeration of the sample chambers for long-term storage. These may be addressed in future iterations by lyophilizing the magnetic

beads directly in the sample chamber, enabling direct rehydration with the blood sample, and allowing for long-term storage and transport in variable field conditions. Cost is also a limitation, notably antibody-functionalized magnetic beads, although costs are expected to decrease with manufacturing at scale through bulk synthesis and conjugation; we estimate future per-sample costs to be on the order of ~$2 (~$1.19 per sample for antibody beads, Table S2), which is appropriate for near-patient viral load testing in decentralized clinics (*e.g.*, GeneXpert, ~$20–30 per test)[43] and centralized assays such as clinical chemistry panels and liquid biopsy (which cost tens to thousands of dollars).[44] Future work will focus on further reducing per-assay processing costs, scaling the platform to accommodate different sample volumes, mitigating potential DNA loss by exploring membrane surface modifications, incorporating blocking agents such as BSA, and evaluating alternative materials with reduced nucleic acid-binding affinity. Finally, demonstrating the battery-powered operation of the micropump will expand the potential POC use to field settings without grid-based power.

Conclusions

PlasmaLIFT offers an automated, centrifuge-free method for processing clinically relevant blood volumes (up to 5 mL) at the point of care. Its performance is comparable to traditional lab methods such as centrifugation. Its scalability, modularity, and ease of use make it a promising tool for expanding access to vital blood diagnostics in decentralized environments, either as a standalone tool for plasma separation or integrated with microfluidic nucleic acid extraction or amplification devices for sensitive assays such as liquid biopsies.

Experimental section

Collection and storage of human whole blood

Healthy control human whole blood was purchased from HumanCells Biosciences; all specimens were de-identified and tested negative for HIV1/2, HBV, HCV, and syphilis prior to receipt. Whole blood was stored at 4 °C and handled using BSL-2 facilities and protocols. Blood samples were used within 48 hours of receipt.

Design and fabrication of PlasmaLIFT device

The disposable sample chamber, magnet holder, and filter cap components were designed in Fusion 360 and 3D printed in VeroWhite resin (Stratasys Objet30). Printed parts were cleaned in an alkaline bath for 5 h, rinsed, and dried at 30 °C for ≥2 h. The chamber's internal dimensions were 34 × 24 × 10 mm with 1 mm walls. For the magnet holder, 7/16″ × 1/2″ N52 neodymium disc magnets (D78-N52, K&J Magnetics) were inserted and secured with light-cure adhesive (Loctite 3525), then cured with 3000 flashes in a UV unit (Otoflash G171).

The filter cap lid, inlet, and outlet were also 3D printed. The inlet included a rectangular seal between the filter cap and the lid to prevent leakage, and both inlet/outlet surfaces incorporated a ringed spoke pattern to distribute fluid across the membranes. Square-profile O-rings (11 mm ID, 1171 N102, McMaster-Carr) were installed into the inlet and outlet pieces. Glass fiber membranes (2.7 μm APFD02500; 0.7 μm APFF04700, Millipore) were punched to 14.29 mm diameter and stacked with the 2.7 μm membrane facing the inlet. Assembled pieces were edge-sealed with light-cure adhesive and UV-cured (3000 flashes).

Steel tube fittings were added for pump interfacing. A 2.5 mm segment of 23G tubing (5560 K651, McMaster-Carr) was inserted into the inlet and then bent 90° toward the chamber front (such that the length of the tubing was 2.25 mm from the edge of the filter cap). Pre-cut 23G tubing (LVF-KFI-13, Darwin Microfluidics) was inserted into the outlet. Both were sealed with light-cure adhesive and UV-cured. Filter caps were connected to a miniature peristaltic pump (CPP-11000-ZM, Jobst Technologies) using 1/16″ OD PTFE tubing (BL-PTFE-1605-20, Darwin Microfluidics). The peristaltic pump enables bidirectional fluid pumping with flow rates ranging from 5 μL min^{-1} to 1600 μL min^{-1}, linearly proportional to the applied voltage (3.3 V max), and is 9.5 × 11.2 × 40.5 mm in size. Tubing was inserted into the inlet steel fitting and the pump inlet. Pump voltage and timing were controlled *via* the manufacturer's software (JT-Pump-Driver, Jobst Technologies, Github).

Initial testing of PlasmaLIFT

To establish proof-of-concept for PlasmaLIFT, we first assessed the feasibility for combining immunomagnetic depletion and dual membrane filtration for improving blood processing capacity. RBC depletion magnetic particles (EasySep RBC Depletion Reagent, StemCell Technologies, purchased commercially for $12.50 for each 5 mL of whole blood) were added to 5 mL whole blood at 100 μL mL^{-1} (500 μL total) in a 5 mL centrifuge tube, mixed by gentle inversion, and placed on a magnetic separator (MSR8X5, Permagen Labware). After 5 min, the supernatant was carefully removed without disturbing the RBC pellet and transferred to a clean tube. This supernatant was drawn into a 3 mL syringe, passed through the dual-membrane filter, and the filtrate was collected in a 5 mL tube. For filtration-only controls, whole blood was directly loaded into the filter using a syringe.

Finite-element modeling of device-generated magnetic fields

Finite element modeling of device-generated magnetic fields was performed in COMSOL Multiphysics (Magnetic Fields, No Currents module). Simulations used N52 sintered neodymium disc magnets with dimensions and arrangements matching each experimental configuration. Magnetic flux density and field lines were visualized to assess field strength and spatial distribution. Simulated field profiles were qualitatively compared with experimental RBC separation behavior to

evaluate agreement between modeled and observed magnetic effects.

Automated device operation and workflow

For PlasmaLIFT separation, 5 mL whole blood was added to the sample chamber containing RBC depletion magnetic particles (EasySep, StemCell Technologies) at 100 μL mL^{-1} (500 μL total). After inserting the filter cap, the chamber was inverted for 5–10 s and placed on the magnetic separator. The pump tubing was attached, and after 6 min of magnetic separation the RBC-depleted supernatant was pumped through the filter cap at 1.8 V (≈557 μL min^{-1}), collecting cell-free plasma in a 5 mL tube. The pump was stopped after 4 min.

Optimization of immunomagnetic separation workflow

To assess its effects on magnetic separation efficiency, bead volume was varied from 50–150 μL mL^{-1}, with each sample mixed for 5 s. After 5 minutes of magnetic separation, the RBC-depleted supernatant was carefully collected without disturbing the pellet, and its volume was measured. For mixing-time optimization, bead volume was fixed at 100 μL mL^{-1}, and samples were mixed for 5, 10, or 30 s. Following 5 min of separation, the supernatant volume was measured. To optimize separation time, bead volume (100 μL mL^{-1}) and mixing time (5 s) were held constant, and separation durations of 3–6 min were tested before supernatant extraction and measurement.

Optimization of immunomagnetic separation combined with filtration

Flow rate effects were assessed by varying the peristaltic pump voltage from 1.2 to 3.0 V, producing flow rates of 335 to 960 μL min^{-1}. Flow rates were calibrated by measuring the volume of PBS passing through the filter over 30 s and converting to μL min^{-1}. Filter diameter was fixed at 14.29 mm. Bead volume was held at 100 μL mL^{-1}, and samples were mixed for 10 s. After 6 min of magnetic separation, the RBC-depleted supernatant was withdrawn through the filter cap at each flow rate, and the recovered plasma volume was measured.

To evaluate the filter diameter, filter caps ranging from 12.7 to 25.4 mm were fabricated. Bead volume was fixed at 100 μL mL^{-1}, and samples were mixed for 5 s. Following a 6-minute separation, the supernatant was removed through each filter at a rate of 557 μL min^{-1}, and the recovered plasma volume was measured.

Transmembrane pressure across the filtration membrane was measured using an Elveflow microfluidic inline pressure sensor (MFP) connected to an Elveflow OB1 flow controller. A positive-pressure configuration was used, as the sensor cannot measure negative pressures. RBC-depleted supernatant was pumped through the system using the peristaltic pump, passing first through the pressure sensor, then through the 14.3 mm dual membrane filter cap, and finally into an empty collection tube. Pressure was continuously recorded at 1.8 V (557 μL min^{-1} flow rate), and data were plotted as transmembrane pressure *versus* time to characterize flow resistance during operation. The outlet pressure was assumed to be standard atmospheric pressure.

Evaluation of cell separation efficiency and hemolysis

Gold-standard controls were centrifuged at 1500× g for 10 min, and plasma was carefully transferred to a clean 5 mL tube. For cell counting, 10 μL of each device-processed or centrifuged sample was mixed 1 : 1 with Trypan Blue (20 μL total) and loaded onto a cell counting slide (C10228, ThermoFisher). Whole blood input samples were diluted 1000-fold before Trypan Blue addition. Cell counts were obtained using an automated counter (Invitrogen Countess 3, ThermoFisher Scientific).

The degree of hemolysis was determined by measuring the absorbance of each sample separated using the device and centrifugation at 414 nm, a known absorbance peak of oxyhemoglobin, using a NanoDrop One spectrophotometer (ThermoFisher Scientific). Plasma obtained using centrifugation and fully lysed whole blood samples were used as controls.

Evaluation of plasma separation across a range of hematocrit levels

To test PlasmaLIFT across blood volumes and hematocrits, whole blood was centrifuged at 1500× g for 10 min. Plasma was removed to measure packed cell volume (>99% RBCs) and then added back to achieve target hematocrits of 40%, 45%, 50%, and 55%.

Protein, metabolite, and lipid quantification

Protein recovery was assessed using the Qubit Protein Assay (Q33211, Invitrogen). Plasma separated by PlasmaLIFT or centrifugation was diluted 100-fold in PBS, mixed with Qubit working solution, and measured on a Qubit 4 Fluorometer.

Glucose recovery was evaluated with the Glucose Colorimetric Detection kit (EIAGLUC, Invitrogen). Plasma, collected ~48 h post-collection, was diluted 20-fold in assay buffer, and absorbance at 560 nm was measured in a microplate reader. Concentrations were interpolated from a 4-parameter sigmoidal standard curve.

Total cholesterol was measured using the Total Cholesterol Colorimetric Assay kit (EEA026, Invitrogen) on undiluted plasma. Absorbance at 510 nm was read in a microplate reader, and cholesterol was calculated per kit instructions.

Nucleic acid quantification

Endogenous DNA yield was measured using the Qubit 1× dsDNA HS Assay kit (Q33231, Invitrogen) following cfDNA extraction from 1 mL plasma with the MAGicBead™ cfDNA Isolation kit (D4086, Zymo Research). DNA standards and samples were combined with 1× dsDNA working solution and read on a Qubit 4 Fluorometer.

For spiked DNA recovery, a 179-bp lambda fragment was added to 5 mL whole blood at 4000 copies per mL before plasma separation. DNA was extracted from 1 mL plasma, and qPCR was performed using PowerTrack SYBR Green Master Mix (1×), 400 nM primers (forward: 5′-CGGCATTCGGC AGATATT-3′, reverse: 5′-CAACGGCAATACACACATTAC-3′), in a 20 μL reaction on a QuantStudio 3 thermocycler (95 °C 2 min; 50 cycles of 95 °C 5 s, 60 °C 15 s). Reactions were run in triplicate, and Ct values were averaged.

For miRNA recovery, synthetic cel-miR-39 was spiked into whole blood at 10^6 copies per mL. RNA was extracted from 150 μL plasma using the Quick-DNA/RNA Miniprep Kit (D7001, Zymo Research) and converted to cDNA using the microScript microRNA cDNA Synthesis kit. qPCR was performed with PowerTrack SYBR Green Master Mix, 1 μL cel-miR-39 forward primer, and 1 μL Universal miRNA Reverse Primer on a QuantStudio 3 (95 °C 3 min; 50 cycles of 94 °C 15 s, 60 °C 30 s) in triplicate, and Ct values were averaged.

Spike-in virus quantification

Inactivated HCV (NATHCV-0005, Zeptometrix) was spiked into whole blood at 150 IU mL^{-1}. Following plasma separation, viral RNA was extracted from 280 μL plasma using the Qiagen Viral RNA Mini kit (52 904, Qiagen). HCV RNA was amplified using previously published primers and probe (MAD-1: 5′-TGCTAG CCGAGTAGYGTTGG-3′; MAD-2: 5′-ACTCGCAAGCACCCTATCAG-3′; MAD-3 probe: 5′-ACCACAAGGCCTTTCGCGAC-3′).[45] RT-qPCR was performed in 20 μL reactions with PrimeScript One-Step RT-PCR Master Mix (1×), 500 nM primers, and 125 nM probe on a QuantStudio 3 thermocycler (52 °C 5 min; 95 °C 10 s; 50 cycles of 95 °C 5 s, 60 °C 30 s). Reactions were run in triplicate and Ct values averaged.

Statistics

All statistical analyses were performed using Graphpad Prism 10. Welch's unpaired *t*-tests were used for comparisons between two groups. One-way ANOVA was used for analysis across multiple groups. *Post hoc* multiple comparisons were performed when necessary using one-way ANOVA Tukey's multiple comparisons test. Simple linear regression analysis was performed when determining statistically significant correlation between variables.

Live subject statement

All blood samples used were purchased as de-identified specimens from HumanCells Biosciences. All human blood samples were collected by HumanCells Biosciences from fully consented, IRB-approved donors who had tested negative for HIV-1/2, HBV, HCV, and syphilis, under IRB #2023-0213, approved by Pearl IRB, in adherence with Good Clinical Practices outlined by the U.S. Food and Drug Administration.

Author contributions

Conceptualization: CMV, BAC, AGA, SKS. Methodology: CMV, BAC, AGA, KAH, SKS. Investigation: CMV, BAC. Visualization: CMV. Funding acquisition: CMV, AGA, SKS. Project administration: CMV. Supervision: CMV, SKS. Writing – original draft: CMV. Writing – review & editing: CMV, BAC, AGA, KAH, SKS.

Conflicts of interest

All authors declare that they have no competing interests.

Data availability

The data supporting this article have been included as part of the supplementary information (SI).

Supplementary information: Comparison of current plasma separation devices for point-of-care applications (Table S1), Magnetic field simulations compared to observed RBC separation for three magnetic separator prototypes (Fig. S1), Quantitative analysis of RBC-depleted supernatant recovery and cell separation efficiency of magnetic separator prototypes (Fig. S2), Transmembrane pressure buildup during filtration (Fig. S3), Top and side views of PlasmaLIFT setup, with smartphone for scale to demonstrate small device footprint (Fig. S4), Projected Per-Sample Cost of Immunomagnetic RBC Depletion at Manufacturing Scale (Supp. Materials and Methods). See DOI: https://doi.org/10.1039/d6lc00135a.

Acknowledgements

This work was supported by the National Science Foundation Graduate Research Fellowship under Grant No. DGE 2036197 (CMV) and NIH R01AI188944.

References

1 M. Kersaudy-Kerhoas and E. Sollier, Micro-scale blood plasma separation: from acoustophoresis to egg-beaters, *Lab Chip*, 2013, **13**, 3323–3346.
2 H. Yuan, P.-Y. Chiu and C.-F. Chen, Paper-based analytical devices for point-of-care blood tests, *Biomicrofluidics*, 2021, **15**, 041303.
3 O. G. Chavez-Pineda, *et al.*, Microfluidic systems for the analysis of blood-derived molecular biomarkers, *Electrophoresis*, 2022, **43**, 1667–1700.
4 M. Lee, *et al.*, Advances in Whole Blood Separation Techniques for Point-of-Care Testing, *ACS Sens.*, 2025, **10**(12), 9203–9224.
5 L. M. Rey Gomez, R. Hirani, A. Care, D. W. Inglis and Y. Wang, Emerging microfluidic devices for sample preparation of undiluted whole blood to enable the detection of biomarkers, *ACS Sens.*, 2023, **8**, 1404–1421.
6 J. Cadamuro, *et al.*, Influence of centrifugation conditions on the results of 77 routine clinical chemistry analytes using standard vacuum blood collection tubes and the new BD-Barricor tubes, *Biochem. Med.*, 2018, **28**, 010704.

7 D. Lesche, *et al.*, Does centrifugation matter? Centrifugal force and spinning time alter the plasma metabolome, *Metabolomics*, 2016, **12**, 159.
8 M. E. Haque, *et al.*, A low-cost, open-source centrifuge adaptor for separating large volume clinical blood samples, *PLoS One*, 2022, **17**, e0266769.
9 W. S. Mielczarek, E. A. Obaje, T. T. Bachmann and M. Kersaudy-Kerhoas, Microfluidic blood plasma separation for medical diagnostics: is it worth it?, *Lab Chip*, 2016, **16**, 3441–3448.
10 R. Salomon, *et al.*, Challenges in blood fractionation for cancer liquid biopsy: how can microfluidics assist?, *Lab Chip*, 2025, **25**, 1097–1127.
11 Cepheid-Xpert-HIV-1-VL-XC-GPM-Reference-Sheet-A4-CE-IVD-3359-English, https://cepheid.widen.net/view/pdf/ygaambrv4z/Cepheid-Xpert-HIV-1-VL-XC-GPM-Reference-Sheet-A4-CE-IVD-3359-English.pdf?.
12 J. A. Sacks, *et al.*, Performance of Cepheid Xpert HIV-1 viral load plasma assay to accurately detect treatment failure, *AIDS*, 2019, **33**, 1881–1889.
13 A. C. Guimarães, M. Wolfart, M. L. L. Brisolara and C. Dani, Causes of rejection of blood samples handled in the clinical laboratory of a University Hospital in Porto Alegre, *Clin. Biochem.*, 2012, **45**, 123–126.
14 M. H. Kroll and R. J. Elin, Interference with clinical laboratory analyses, *Clin. Chem.*, 1994, **40**, 1996–2005.
15 B. Ünlü, *et al.*, Effect of blood cell subtypes lysis on routine biochemical tests, *J. Med. Biochem.*, 2018, **37**, 67–77.
16 M. Turchiano, C. Nguyen, A. Fierman, M. Lifshitz and A. Convit, Impact of blood sample collection and processing methods on glucose levels in community outreach studies, *J. Environ. Public Health*, 2013, **2013**, 256151.
17 L. M. Mikesh and D. E. Bruns, Stabilization of glucose in blood specimens: mechanism of delay in fluoride inhibition of glycolysis, *Clin. Chem.*, 2008, **54**, 930–932.
18 M. K. Tuck, *et al.*, Standard operating procedures for serum and plasma collection: early detection research network consensus statement standard operating procedure integration working group, *J. Proteome Res.*, 2009, **8**, 113–117.
19 E. P. Erdal, D. Mitra, V. S. Khangulov, S. Church and E. Plokhoy, The economic impact of poor sample quality in clinical chemistry laboratories: results from a global survey, *Ann. Clin. Biochem.*, 2017, **54**, 230–239.
20 M. Kaisar, *et al.*, Plasma degradome affected by variable storage of human blood, *Clin. Proteomics*, 2016, **13**, 26.
21 M. Rózga, T. Bittner, R. Batrla and J. Karl, Preanalytical sample handling recommendations for Alzheimer's disease plasma biomarkers, *Alzheimers Dement*, 2019, **11**, 291–300.
22 J. H. Son, *et al.*, Hemolysis-free blood plasma separation, *Lab Chip*, 2014, **14**, 2287–2292.
23 P. Ďurč, F. Foret and P. Kubáň, Fast blood plasma separation device for point-of-care applications, *Talanta*, 2018, **183**, 55–60.
24 H. T. Ngo, *et al.*, Sensitive and Quantitative Point-of-Care HIV Viral Load Quantification from Blood Using a Power-Free Plasma Separation and Portable Magnetofluidic Polymerase Chain Reaction Instrument, *Anal. Chem.*, 2023, **95**, 1159–1168.
25 S. Yang, A. Undar and J. D. Zahn, A microfluidic device for continuous, real time blood plasma separation, *Lab Chip*, 2006, **6**, 871–880.
26 H. Madadi, J. Casals-Terré and M. Mohammadi, Self-driven filter-based blood plasma separator microfluidic chip for point-of-care testing, *Biofabrication*, 2015, **7**, 025007.
27 C. Gilroy, *et al.*, A passive blood separation sensing platform for point-of-care devices, *npj Biosensing*, 2025, **2**, 19.
28 A. Haller, *et al.*, Microfluidic Vortex Enhancement for on-Chip Sample Preparation, *Micromachines*, 2015, **6**, 239–251.
29 J. Marchalot, Y. Fouillet and J.-L. Achard, Multi-step microfluidic system for blood plasma separation: architecture and separation efficiency, *Microfluid. Nanofluid.*, 2014, **17**, 167–180.
30 A. Nabatiyan, Z. A. Parpia, R. Elghanian and D. M. Kelso, Membrane-based plasma collection device for point-of-care diagnosis of HIV, *J. Virol. Methods*, 2011, **173**, 37–42.
31 W. Brakewood, K. Lee, L. Schneider, N. Lawandy and A. Tripathi, A capillary flow-driven microfluidic device for point-of-care blood plasma separation, *Front. Lab Chip Technol.*, 2022, **1**, 1051552.
32 L. Xu, *et al.*, Phaseguide-assisted blood separation microfluidic device for point-of-care applications, *Biomicrofluidics*, 2015, **9**, 014106.
33 N. Debnath, L. S. Live and M. Poudineh, A microfluidic plasma separation device combined with a surface plasmon resonance biosensor for biomarker detection in whole blood, *Lab Chip*, 2023, **23**, 572–579.
34 B. Xu, *et al.*, High-performance blood plasma separation based on a Janus membrane technique and RBC agglutination reaction, *Lab Chip*, 2022, **22**, 4382–4392.
35 X. Su, *et al.*, High-Efficiency Plasma Separator Based on Immunocapture and Filtration, *Micromachines*, 2020, **11**(4), 352.
36 C. Liu, *et al.*, A high-efficiency superhydrophobic plasma separator, *Lab Chip*, 2016, **16**, 553–560.
37 C. Liu, *et al.*, Membrane-based, sedimentation-assisted plasma separator for point-of-care applications, *Anal. Chem.*, 2013, **85**, 10463–10470.
38 X. Qiu, *et al.*, A plasma separator with a multifunctional deformable chamber equipped with a porous membrane for point-of-care diagnostics, *Analyst*, 2020, **145**, 6138–6147.
39 A. G. Ayers, C. M. Victoriano and S. K. Sia, Integrated device for plasma separation and nucleic acid extraction from whole blood toward point-of-care detection of bloodborne pathogens, *Lab Chip*, 2024, **24**, 5124–5136.
40 S. Vemulapati and D. Erickson, Portable Resource-Independent Blood-Plasma Separator, *Anal. Chem.*, 2019, **91**, 14824–14828.
41 S. Vemulapati and D. Erickson, H.E.R.M.E.S: rapid blood-plasma separation at the point-of-need, *Lab Chip*, 2018, **18**, 3285–3292.
42 W. H. Reinhart, The optimum hematocrit, *Clin. Hemorheol. Microcirc.*, 2016, **64**, 575–585.
43 L. Puri, C. Oghor, C. M. Denkinger and M. Pai, Xpert MTB/RIF for tuberculosis testing: access and price in highly privatised health markets, *Lancet Global Health*, 2016, **4**, e94–e95.

44 D. Sánchez-Calderón, *et al.*, Analysis of the Cost-Effectiveness of Liquid Biopsy to Determine Treatment Change in Patients with Her2-Positive Advanced Breast Cancer in Colombia, *Clin. Outcomes Res.*, 2020, **12**, 115–122.

45 D. Candotti, J. Temple, F. Sarkodie and J.-P. Allain, Frequent recovery and broad genotype 2 diversity characterize hepatitis C virus infection in Ghana, West Africa, *J. Virol.*, 2003, **77**, 7914–7923.